Toward the Elucidation of the Structural Determinants Responsible for the Molecular Recognition between Mad1 and Max†

Martin Montagne,‡ Jean-François Naud,§ François-Olivier McDuff,‡ and Pierre Lavigne*,‡

Département de Pharmacologie, Département de microbiologie et d'infectiologie, Faculté de médecine, Université de Sherbrooke, Sherbrooke, Québec J1H 5N4, Canada

Received January 13, 2005; Revised Manuscript Received May 30, 2005

ABSTRACT: Mad1 is a member of the Mad family. This family is part of the larger Myc/Max/Mad b-HLH-LZ eukaryotic transcription-factor network. Mad1 forms a specific heterodimer with Max and acts as a transcriptional repressor when bound to an E-box sequence (CACGTG) found in the promoter of c-Myc target genes. Mad1 cannot form a complex with DNA by itself under physiological conditions. A global model for the molecular recognition has emerged in which the Mad1 b-HLH-LZ homodimer is destabilized and the Mad/Max b-HLH-LZ heterodimer is favored. The detailed structural determinants responsible for the molecular recognition remain largely unknown. In this study, we focus on the elucidation of the structural determinants responsible for the destabilization of the Mad1 b-HLH-LZ homodimer. Conserved acidic residues at the dimerization interface (position a) of the LZ of all Max-interacting proteins have been hypothesized to be involved in the destabilization of the homodimeric states. In Mad1, this position corresponds to residue Asp 112. As reported for the complete gene product of Mad1, we show that wild-type b-HLH-LZ does not homodimerize or bind DNA under physiological conditions. On the other hand, the single mutation of Asp 112 to an Asn enables the b-HLH-LZ to dimerize and bind DNA. Our results suggest that Asp 112 is implicated in the destabilization of Mad1 b-HLH-LZ homodimer. Interestingly, this side chain is observed to form a salt bridge at the interface of the LZ domain in the crystal structure of Mad1/Max heterodimeric b-HLH-LZ bound to DNA [Nair, S. K., and Burley, S. K. (2003) *Cell 112*, 193−205]. This clearly suggests that Asp 112 plays a crucial role in the molecular recognition between Max and Mad1.

The Myc/Max/Mad network plays a key role in the regulation of cell growth, proliferation, differentiation, and apoptosis (*1*, *2*). This network includes Max, the Myc family (c-Myc, *N*-Myc, and L-Myc), and the Mad family [Mad1, Mad2 (Mxi1), Mad3, and Mad4]. As a heterodimer with Max, these proteins control the transcription of numerous genes, often referred to as Myc target genes (*3*, *4*). Max is therefore the central protein of this network. Besides its demonstrated ability to bind to E-box sequences as a homodimer *in vitro*, the major role of Max is believed to be the heterodimeric partner of the other proteins in the network (*5*, *6*). The binding of the heterodimers to E-box sequences, in the promoters of Myc target genes, modulates their transcription (*7*−*9*). For example, the c-Myc/Max heterodimer transactivates Myc target genes by recruiting protein complexes with histone acetyl transferase (HAT) activity. The recruitment of the HAT activity proteins proceeds via the conserved N-terminal Myc boxes (MBI and MBII) in the transactivating domain (TAD) (*10*). Acetylation of histones leads to the opening of the chromatin in the vicinity of target gene promoters, which in turn allows the transcriptional initiation complex formation (*11*). Conversely, Mad/Max heterodimers repress transcription, by recruiting protein complexes with histone deacetylase (HDAC) activity (*12*). The deacetylation of histones closes the chromatin and prevents the transcriptional complex formation. HDAC complexes are recruited by the mSin3-interacting domain (SID), located in the N-terminal portion of Mad proteins (*13*, *14*). Numerous proteins have been identified in these complexes, such as mSin3, N-CoR, SAP30, HDAC1, and HDAC2 (*13*, *14*).

As for all of the proteins known to interact with Max, Mad1 cannot form a homodimer or bind DNA on its own (*15*). Destabilization of the homodimer is thought to be a prerequisite for the specific heretodimerization with Max. The HLH-LZ is known to be responsible for the heterodimeric recognition and dimerization (*5*). Therefore, the molecular determinants for the preferential heterodimerization, for the stabilization of the heterodimer and the concomitant destabilization of the homodimeric Mad1, are likely embedded at the interface of the HLH-LZ domains (*16*−*18*). Interestingly, acidic side chains are strictly conserved at a specific position a (112 in Mad1) in the LZ domains of all of the known interacting partners (Figure 1a)

† This study was supported by the Canadian Institutes of Health Research (CIHR) (Grant MOP-121408). Pierre Lavigne acknowledges the Fonds de la Recherche en Santé du Québec (FRSQ) for a scholarship.

* To whom correspondence should be addressed: Département de Pharmacologie, Faculté de médecine, Université de Sherbrooke, 3001 12e ave nord, Fleurimont, Québec J1H 5N4, Canada. Telephone: 819-820-6868 ext. 15462. Fax: 819-564-5400. E-mail: pierre.lavigne@usherbrooke.ca.

‡ Département de Pharmacologie.

§ Département de microbiologie et d'infectiologie.

10.1021/bi0500731 CCC: $30.25
Published on Web 09/02/2005

a)

LEUCINE ZIPPER

Max	MRRKNHT**H**QQDIDD**L**KRQNAL**L**EQQVRA**L**EK
c-Myc	VQAE**E**QKLISFEDL**L**RKRREQ**L**KHKLEQ**L**RN
Mad1	LEDC**D**RKAVHQIDQ**L**QREQRH**L**KRQLEK**L**GI
Mxi1	LEEA**E**RKSQHQLEN**L**EREQRF**L**KWRLEQ**L**QG
Mad4	LEEQ**D**RRALSIKEQ**L**QQEHRF**L**KRRLEQ**L**SV
N-Myc	LQAE**E**HQLLLEKEK**L**QARQQQ**L**LKKIEHART
L-Myc	LVGA**E**KRMATEKRQ**L**RCRQQQ**L**QKRIAY**L**SG

b)

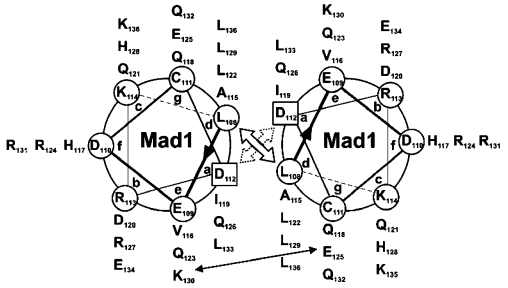

c)

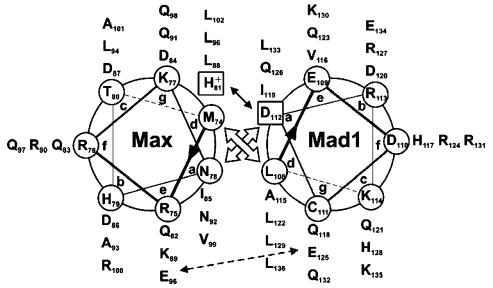

FIGURE 1: (a) Amino acid sequence alignment of the LZ domains of Myc/Max/Mad family members. Conserved acidic residues at positions a and leucine residues at position d are displayed in bold. Also shown in bold is the histidine residue 81 d of Max. Helical wheel representation of the Mad1/Mad1 homodimeric (b) and Mad1/Max heterodimeric LZ (c). The dashed and straight lines show the unfavorable and favorable interhelical salt bridges, respectively.

(*16*−*18*). This has led to the hypothesis that these interfacial acidic side chains (Glu/Asp) are involved in the destabilization of Myc and Mad homodimers (Figure 1b) (*16*−*18*). We have also proposed that the conserved Glu 407 a and Glu 414 a in c-Myc could form a stable salt bridge with a particular His side chain at position 81 d in the Max LZ. The existence of a stable salt bridge was confirmed by the measurement of an elevated pK_a of the His side chain in the heterodimeric c-Myc/Max LZ (*16*). The existence of this interaction was further confirmed from the heterodimeric LZ NMR solution structure (*17*). The exact same interaction can be observed in the crystal structure of c-Myc/Max b-HLH-LZ with DNA (*19*). Interestingly, in the crystal structure of Mad1/Max b-HLH-LZ/E-box, the equivalent specific salt bridge between Asp 112 a and His 81 d can clearly be observed. On the other hand, it was alternately proposed that a network of favorable hydrogen bonds, formed by a tetrad between Glu 125 g and Gln 126 a of Mad1 and Gln 91 g and Asn 92 a at the interface of Max, was responsible for molecular recognition (*19*). In light of the macroscopic mechanism of molecular recognition, they proposed that the replacement of Glu 125 g by a Gln was enough to disrupt molecular recognition by the removal of a destabilizing charge at the interface of a putative Mad1 homodimeric b-HLH-LZ. Concurrently, it is possible that alternate and/or concomitant determinants involving Glu 125 g and/or Asp 112 a exist for the destabilization of Mad1 homodimeric b-HLH-LZ and for the stabilization of the heterodimer as shown in Figure 1c.

In this context, we have studied the dimerization and DNA binding of the b-HLH-LZ of Mad1 (Mad1*WT) and of one mutant (D112N or Mad1*DN). We show that no apparent dimerization of the Mad1*WT is detected at neutral pH. On the other hand, we observe that it can form a homodimer with an apparent K_D of 9.28×10^{-7} at pH 2.8 and 20 °C, where both Glu 125 g and Asp 112 a should be protonated. To further discriminate between the two acidic side chains, we have mutated Asp 112 to an Asn (Mad1*DN). We show that Mad1*DN forms a homodimer at pH 6.8 with an apparent K_D of 5.83×10^{-6} at 20 °C. In addition, Mad1*DN forms a stable complex with an E-box sequence at 37 °C. Conversely, the Mad1*WT/E-box complex does not appear to exist at this temperature. Therefore, Asp 112 emerges as a crucial residue for the destabilization of Mad1 b-HLH-LZ homodimer and for the preclusion of DNA binding as a homodimer.

EXPERIMENTAL PROCEDURES

*Construction of pET3a Expression Plasmids Encoding Mad1*WT and Mad1*DN.* The DNA coding for the b-HLH-LZ of Mad1 (residues 57S−136L) was amplified by a polymerase chain reaction (PCR) from pME18S-Mad1 (kindly provided by R. N. Eisenman, Fred Hutchinson Cancer Research Center, Seattle, WA) using the following oligonucleotides 5′-d(CCCGGCGGCATATGAGCAGATCAACTCACAATGAA)-3′ and 5′-d(GCCGGATCCGCCCAGCTTCTCCAGCTGCCTCTT)-3′, as 5′ and 3′ primers that contain *Nde*I and *Bam*HI restriction sites, respectively, for cloning into the pET3a plasmid (Novagen). No stop codon was used. This resulted in a C-terminal extension of GSGC. Cysteines 75 and 111 were mutated to serines by site-directed PCR mutagenesis to obtain Mad1*WT. The D112N mutant (Mad1*DN) was generated by site-directed PCR mutagenesis from Mad1*WT.

Protein Expression and Purification. The expression pET3a plasmids containing Mad1*WT and Mad1*DN were transformed into *Escherichia coli* strain BL21 AI (Novagen), plated on LB-agar-containing ampicillin (Amp), and grown at 37 °C overnight. Precultures from single colonies were grown in 10 mL of LB until an optical density (OD_{595}) of 0.6 at 595 nm was reached. Then 1 L of LB-containing Amp was inoculated with precultures and grown at 37 °C until an OD_{595} of 0.6 was reached. The expression of the proteins was induced by the addition of 2% L-arabinose for 4 h. After induction, cells were harvested by centrifugation and the pellets were suspended in 10 mL of suspension buffer (50 mM HEPES-NaOH (pH 7.5), 0.1 M NaCl, 10 mM $MgCl_2 \cdot 6H_2O$, and 5 mM DTT. The suspension was incubated with agitation at 30 °C for 30 min. A final concentration of 1% of Triton X-100 was added to the suspension prior to sonication on ice. The lysate was centrifuged at 30 000*g* for 30 min at 4 °C to harvest the inclusion bodies containing Mad1*WT and Mad1*DN. Each pellet was resuspended in 15 mL of solubilizing buffer (6 M urea, 100 mM NaAc (pH 5), 0.5 M GuHCl, and 25 mM DTT). An additional 15 mL

of 2 M urea was then added to complete the solubilization. The samples were subjected to a final centrifugation at 30000*g* for 30 min at 4 °C. The supernatant was collected, filtered, and loaded onto HiPrep SP XL (Pharmacia) cation-exchange columns. The Mad1 proteins, once washed with 3 column volumes of buffer A (50 mM sodium acetate at pH 5.0) and 3 column volumes of 90% buffer A/10% buffer B (50 mM sodium acetate and 5 M NaCl), were eluted with a linear NaCl gradient (10−35% buffer B) at 2.5 mL/min. The fractions containing Mad1 were collected, desalted on HiTrap desalting columns, and then lyophilized. Stock solutions were prepared in 50 mM phosphate (pH 6.8 and 2.8), 50 mM KCl, and 5 mM DTT (CD buffer). The stock solution concentration was determined by the Bio-Rad protein assay.

Circular Dichroism (CD). CD measurements were performed on a Jasco J-810 spectropolarimeter equipped with a Jasco Peltier-type thermostat. The instrument was calibrated routinely with an aqueous solution of *d*-10-(+)-camphorsulfonic acid at 290.5 nm. The samples were loaded into quartz cells with a path length of 0.1 cm. Spectra were recorded at 20 °C from 250 to 195 nm by accumulating 10 scans at 0.1 nm intervals. The raw m° values were transformed in mean residue molar ellipticity (deg·cm^2·dmol^{-1}) using the following equation $[\Theta]_{222}$ = CD signal (deg)·MRW/concentration (g/L)·*l*·10, where MRW is the mean residue weight and *l* is the path length of the CD cell. The temperature denaturations (proteins, DNA, and protein−DNA complexes) were performed by monitoring $[\Theta]_{222}$ in a temperature range from 5 to 95 °C at a heating rate of 1 °C/min. The double-stranded E-box DNA (dsDNA) was prepared by heating oligonucleotides containing E-box sequence (underlined) 5′-d(CCCCCAACACGTGTTGCCTGA)-3′ and 5′-d(TCAGGCAACACGTGTTGGGGG)-3′ to 95 °C and cooling the solution slowly to room temperature. The concentration of E-box dsDNA was determined spectrophotometrically at 260 nm. For DNA-binding studies, 20 μM of E-box dsDNA was added to 15 μM of dimer solution. To obtain the effect of DNA onto the conformation and stability of the proteins, its CD spectrum and temperature denaturation were subtracted from those of the corresponding protein/DNA complexes. The concentration dependency of $[\Theta]_{222}$ was monitored by recording the CD spectra of solutions obtained from serial dilution of the stock solution as described above.

Electrophoretic Mobility Shift Assay (EMSA). Radioactive labeling of E-box dsDNA was accomplished by the incubation of T4 polynucleotide kinase with [γ-^{32}P]ATP for 45 min at 37 °C. The purification of ^{32}P-E-box dsDNA was performed on a G-25 column (Pharmacia). A total of 0.2 pmol of radiolabeled E-box dsDNA was added to the proteins, in a 15 μL total reaction buffer containing 20 mM HEPES buffer at pH 7.2, 50 mM KCl, 3 mM $MgCl_2$, 1 mM EDTA, 8% glycerol, 1 mM β-mercaptoethanol, and 10 mM DTT). Additionally, the reaction buffer contained 0.2% NP-40, 0.4 ng of BSA, and 33 ng of nonspecific Herring sperm DNA. This corresponds to a 30-fold excess of nonspecific DNA. The electrophoresis was performed on a 7.5% acrylamide gel at 200 V, at room temperature for 90 min. Gels were then exposed to luminescent photographic film (Kodak).

Molecular Modeling. All of the molecular modeling was done using the InsightII suite (Acceleris) running on an Octane SGI workstation. The protein and DNA coordinates of the Mad1/Max:E-box b-HLH-LZ complex were used (PDB accession number 1AN2) (*20*). Unfolding of the different domains was accomplished through molecular dynamics simulations at high temperature without constraints on the domains to be unfolded. The molecular rendering was done using Ribbons (*21*).

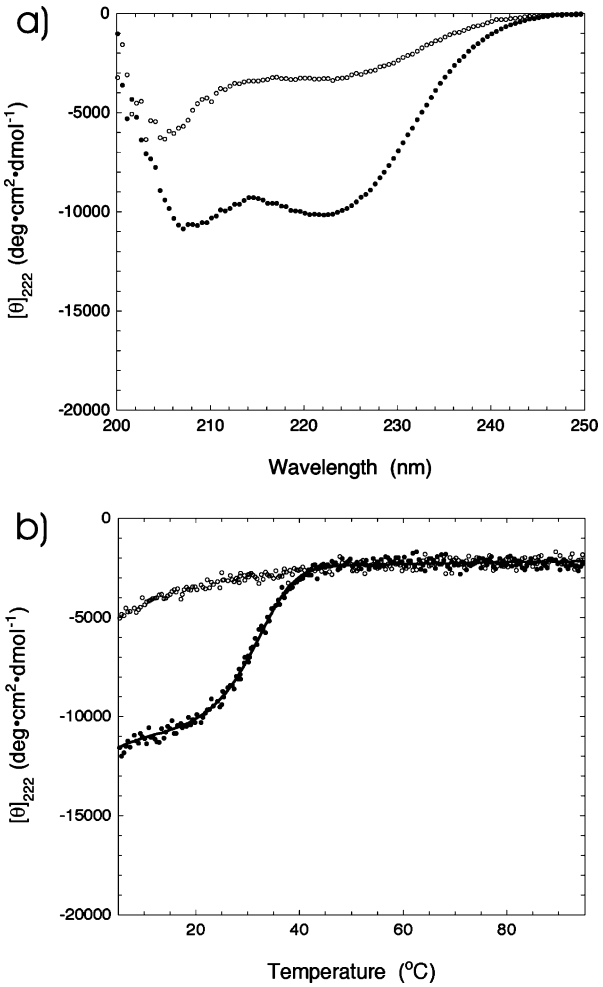

FIGURE 2: (a) Far-UV CD spectra of Mad1*WT recorded at 20 °C and pH 6.8 (○) and pH 2.8 (●). The data are presented in units of mean residual molar ellipticity ([Θ]): deg·cm^2·dmol^{-1}. (b) Temperature-induced denaturation of Mad1*WT at pH 6.8 (○) and pH 2.8 (●) monitored by recording [Θ] at 222 nm as a function of temperature. The protein concentration is 30 μM (monomer units) buffered in CD buffer (50 mM phosphate, 50 mM KCl, and 5 mM DTT). The solid lines in b correspond to the simulation of the denaturation curve.

RESULTS

The b-HLH-LZ of Mad1 Does Not Oligomerize at Neutral pH but Does at pH 2.8. We present in Figure 2a (○), the far-UV CD spectrum of Mad1*WT at 20 °C, 30 μM, and pH 6.8. The spectrum is indicative of a mostly unfolded protein with a residual amount of secondary α-helical content. Indeed, it can be calculated from the $[\Theta]_{222}$ that the α-helical content is approximately 16%. We show in Figure 2b (○) the corresponding temperature denaturation. In accordance with the low amount of α-helical secondary structure, the denaturation depicts a noncooperative transition, suggesting that the b-HLH-LZ of Mad1 has little or no tertiary and/or quaternary interactions at neutral pH. This result is in agreement with the reported fact that the complete

gene product of Mad1 does not homodimerize or bind DNA by itself (*6*) and also supports the existence of destabilizing interactions at the interface of the b-HLH-LZ as proposed previously (*16*, *17*). We present in Figure 1b the putative dimeric interface of Mad1 LZ in a helical wheel representation. As one can observe, one Asp (Asp 112) lies directly at the dimerization interface of the LZ at position a. It has been reported that the presence of an Asp at position a prevents dimerization of highly stable, engineered, and synthetic coiled-coils because of strong electrostatic repulsions and unfavorable desolvation effects of the carboxylate moiety upon burial at the interface (*22*−*24*). It has been proposed (*16*−*17*) that the burial of this acidic residue could only occur if it is engaged in favorable electrostatic interactions with His 81 d of Max as seen in c-Myc/Max heterodimeric LZ (*17*). Interestingly, we see in Figure 1b that Glu 125 g, which has been proposed to be responsible for the instability of Mad1 homodimer (*19*), could possibly be engaged in a favorable interhelical g−e′ salt bridge with Lys 130 e in the homodimer. Additionally, homology modeling of the b-HLH-LZ homodimer reveals that the hydrophobic core of a putative dimeric HLH of Mad1*WT is virtually identical to those of the Mad1/Max (*19*), c-Myc/Max (*19*), and Max/Max (*20*, *25*) dimeric HLH. From this modeling, no residues bearing the same charge are found to be close enough to generate electrostatic repulsions in this domain. On the basis of these findings and observations, we hypothesize that the unfavorable interactions are located in the LZ of Mad1. More specifically, we propose that Asp 112 a is responsible for the observed lack of auto-association of the Mad1*WT at neutral pH.

In this context, we have measured the far-UV CD spectrum (Figure 2a, ●) and monitored the thermal denaturation (Figure 2b, ●) of Mad1*WT at pH 2.8 with the assumption that under such conditions, the acidic side chains should be protonated, the putative interfacial repulsions should be diminished, and the formation of the stable quaternary structure should be induced. As seen in Figure 2a (●), the helical content of Mad1*WT is significantly increased as depicted by a decrease of $[\Theta]_{222}$ from −3 400 to −10 085 deg·cm^2·dmol^{-1} at 20 °C. Moreover, tertiary and quaternary structures are present at pH 2.8, as suggested by the cooperative temperature-induced denaturation in Figure 2b. The $[\Theta]_{222}$ obtained at 20 °C and pH 2.8 (−10 085 deg·cm^2·dmol^{-1}) is about half of that obtained for the engineered and thermodynamically stable b-HLH-LZ of Max, called Max*VL (−22 000 deg·cm^2·dmol^{-1}) (*26*). The NMR solution structure of Max*VL, in absence of DNA, has recently been solved. It was shown that part of the basic region, the H1, H2, and LZ are α-helical (*25*−*26*). Therefore, it is apparent that, at 30 μM and pH 2.8, the b-HLHL-LZ of Mad1 has approximately half (46%) of the secondary structure one would expect for a fully dimeric b-HLH-LZ in the absence of DNA. It is possible that Mad1*WT, under such conditions, exists as a population of 46% of optimally folded b-HLH-LZ, a population of 100% of a dimer with 46% of the optimal helical content, or a weighed average of both scenarios. The first scenario necessitates that the K_D of Mad1*WT should be in the order of 3×10^{-5} at 20 °C and pH 2.8. The second scenario would mean that the dimeric state consists of intermediate states with a quaternary structure composed of either the LZ and part of H2 folded and the HLH unfolded and/or vice versa as shown in Figure 3. We have shown elsewhere that the LZ and HLH of Max can unfold independently and that intermediate states such as those described in Figure 3 coexist in the absence of DNA (*25*).

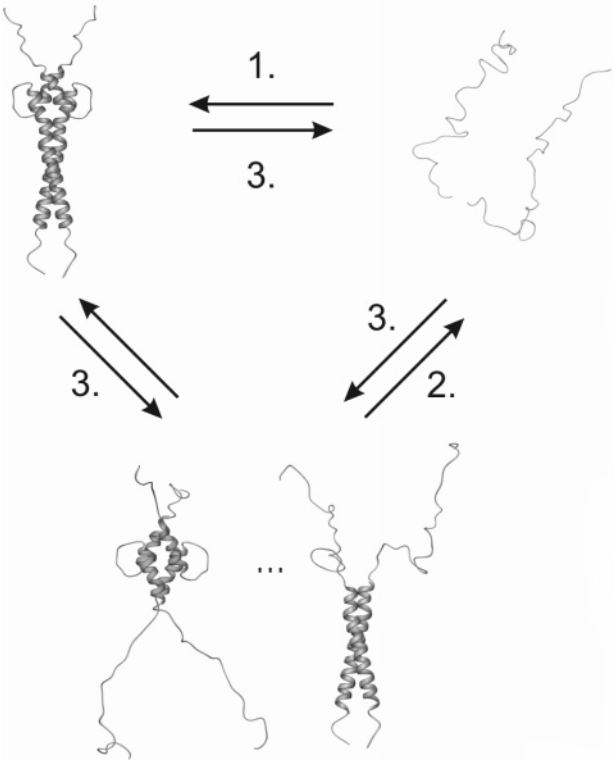

FIGURE 3: Thermodynamical models for the Mad1*WT and Mad1*DN temperature-induced denaturations. (1) Equilibrium between an optimally folded b-HLH-LZ and two denatured monomers. (2) Equilibrium between partially folded dimers (intermediate states) and (3) a combination of both 1 and 2. The models were generated by molecular dynamics simulations and rendered with Ribbons (*21*).

To further characterize the quaternary structure of Mad1*WT and determine the apparent K_D of Mad1*WT at pH 2.8, we have tried to simulate the temperature denaturation curve with three different models, described elsewhere (*26*): (1) the dissociation of fractional population of an optimally folded dimer ($[\Theta]_{222} = -22\,000$ deg·cm^2·dmol^{-1}) into two denatured monomers, (2) the dissociation of a dimer with 50% of the helical content (intermediate states) into two denatured monomers, and finally (3) a combination of models 1 and 2, where the dissociation of a fractional population of an optimally folded dimer can either proceed directly into two denatured monomers or intermediate states with 50% of the optimal helical content. We were not able to fit the thermal denaturation curve with model 1. On the other hand, models 2 and 3 gave essentially identical fits. For the sake of thermodynamical completeness, we favor model 3 that allows for the existence of an optimally folded b-HLH-LZ. While it is impossible at this point to assign a particular structure to the intermediate state or the partially folded dimer, we assume that it consists of an interconverting mixture of states with the LZ and part of H2 folded or states with mostly the HLH folded as depicted in Figure 3. We show in Figure 2b the best fit that we have obtained (—) using model 3. The corresponding and apparent thermodynamical parameters [$T°$, $\Delta H(T°)$, and $\Delta G°$] for the different

Table 1: Thermodynamical Parameters Obtained from the Temperature-Induced Denaturation Simulation of Mad1*WT at pH 2.8[a]

parameters		20 °C	37 °C
T_i°	−3.15 °C		
T_u°	32.40 °C		
ΔH_i°	32.20 kcal/mol		
ΔH_u°	64.25 kcal/mol		
ΔG_u° (kcal/mol)		8.09	5.06
K_D		9.28×10^{-7}	5.73×10^{-4}

[a] These parameters were obtained from the temperature-induced denaturation simulation using model 3 (Figure 2b) and were used to generate the different populations as described elsewhere (*26*) and as shown in Figure 4a.

transitions can be found in Table 1. We present in Figure 4a, the population of the different states as a function of the temperature obtained from the fit. One can see from this figure, that the optimally folded state of Mad1*WT is highly unstable, being only slightly populated (<10%) at low temperature, leaving only the partially folded dimer populated above 5 °C. The corresponding K_D values are 9.28×10^{-7} at 20 °C and 2.73×10^{-4} at 37 °C. As argued above, if we were in the presence of a fractional population (e.g., 50%) of an optimally folded b-HLH-LZ, the corresponding K_D at 20 °C should in the order of 3×10^{-5}. The apparent K_D obtained is 100-fold smaller. This supports the existence of a population of virtually 100% of a partially folded dimer at 20 °C and pH 2.8 for Mad1*WT.

Single Replacement of Asp 112 by an Asn Triggers the Homodimerization of the Mad1 b-HLH-LZ at Neutral pH. To further confirm the implication of Asp 112 in the destabilization of the Mad1 b-HLH-LZ at neutral pH, we replaced it for an Asn to generate the mutant Mad1*DN. This mutation is ideal to verify the effect of the charged side chain of Asp 112. Indeed, the side chain of Asn is isosteric to that of Asp, and the ionizable −OH is replaced by an $-NH_2$. One additional feature of the D112N mutation is that it should prevent the formation of higher order oligomers, such as trimers or tetramers. Indeed, it has been previously shown that the presence of a Asn at position a destabilizes oligomers higher than dimers (*23*, *27*, *28*). On the other hand, an occurrence of a trimeric LZ have been reported to exist despite the presence of an Asn at position a (*29*). Nevertheless, this mutation mimics the local protonation of the $-O^-$ of Asp 112 a at neutral pH, leaving the remaining carboxylates (including Glu 125 g) charged. Therefore, if Asp112 is responsible for most of the unfavorable interactions preventing the Mad1*WT to oligomerize, Mad1*DN should behave similarly to Mad1*WT at pH 2.8.

We present the far-UV CD spectrum obtained at 20 °C in Figure 5a (○) and the thermal denaturation curve of Mad1*DN in Figure 5b (○). The $[\Theta]_{222}$ of −9878 deg·cm^2·dmol^{-1} represents an α-helical content of 44% and is similar to that obtained at pH 2.8 for Mad1*WT. In addition, the temperature-induced denaturation is again cooperative, as for Mad1*WT at pH 2.8, which is indicative of the existence of stable quaternary interactions. We have fitted the temperature denaturation (— in Figure 5b) as described above for Mad1*WT. The apparent thermodynamical parameters are listed in Table 2, and the corresponding populations for the different states are presented in Figure 4b. As for Mad1*WT

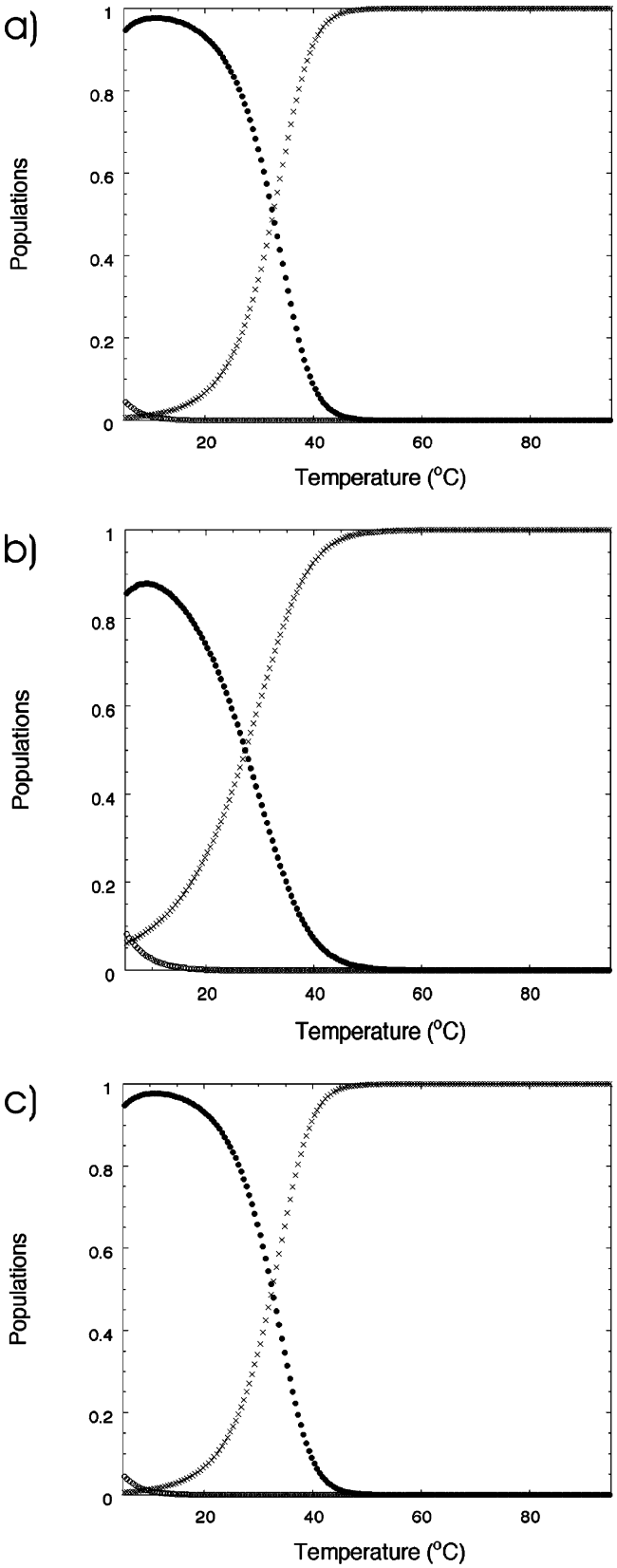

FIGURE 4: Populations of the native (○), intermediate (●), and unfolded (×) states of Mad1*WT at pH 2.8 (a), Mad1*DN at pH 6.8 (b), and Mad1*DN at pH 2.8 (c) in absence of DNA. These populations have been obtained from the thermodynamical parameters listed in Tables 1 and 2.

at pH 2.8, the optimally folded state of Mad1*DN is only slightly populated at low temperatures, with the partially folded dimer being the predominant state at temperatures

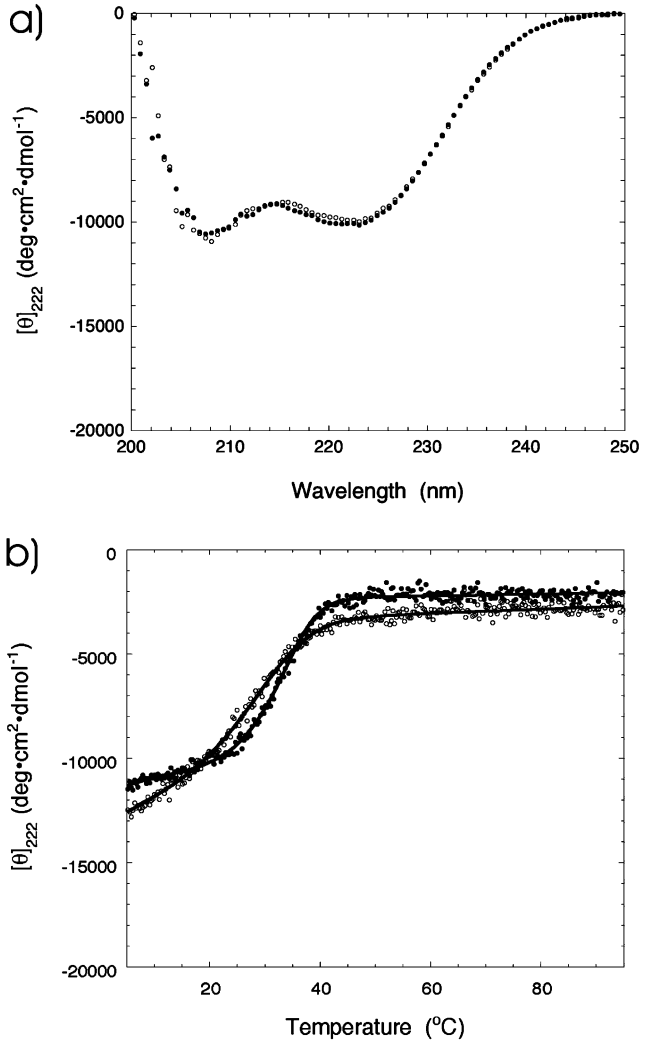

FIGURE 5: (a) Far-UV CD spectra of Mad1*DN recorded at 20 °C and pH 6.8 (○) and pH 2.8 (●). The data are presented in units of mean residual molar ellipticity ([Θ]): deg·cm^2·dmol^{-1}. (b) Temperature-induced denaturation of Mad1*DN at pH 6.8 (○) and pH 2.8 (●) monitored by recording [Θ] at 222 nm as a function of temperature. The protein concentration is 30 μM (monomer units) buffered in CD buffer (50 mM phosphate, 50 mM KCl, and 5 mM DTT). The solid lines in b correspond to the simulation fit of the denaturation curve.

above 5 °C. The corresponding K_D values of this partially folded dimer at pH 6.8 are 5.83×10^{-6} at 20 °C and 3.54×10^{-4} at 37 °C.

To ensure that Mad*DN is a dimer and does not form higher order oligomers, we have simulated the concentration dependence of its $[\Theta]_{222}$ at 20 °C using two-state unfolding models of dimers, trimers, and tetramers. The populations of the unfolded monomer, $P_u(T)$ [or oligomers $(1 - P_u(T))$], are given by the roots [value of P_u as a function of $K_u(T)$ and pt, $P_u(K_u(T),pt$] of the following equations:

$$P_u(T)^2 + \frac{K_u(T)P_u(T)}{4pt} - \frac{K_u(T)}{4pt} = 0 \quad (1)$$

$$P_u(T)^3 + \frac{K_u(T)P_u(T)}{27pt^2} - \frac{K_u(T)}{27pt^2} = 0 \quad (2)$$

$$P_u(T)^4 + \frac{K_u(T)P_u(T)}{256pt^3} - \frac{K_u(T)}{256pt^3} = 0 \quad (3)$$

for the dimer (eq 1), trimer (eq 2), and tetramer (eq 3), respectively. Considering the helical content of Mad1*DN, it is implicit that the oligomers are partially folded and that they can reach a population of 100% at high concentrations. pt is the monomeric protein concentration, and $K_u(T)$ is the two-state equilibrium constant for the unfolding reaction between the oligomers and the unfolded monomers. $K_u(T)$ is classically given by $\exp(-\Delta G_u^\circ(T)/RT)$, where $\Delta G_u^\circ(T)$ is the standard Gibbs free energy of unfolding (standard state of 1 M) and R is the gas constant. $\Delta G_u^\circ(T)$ is given by the Gibbs−Helmholtz equation:

$$\Delta G_u^\circ(T) = \Delta H_u^\circ(T) + \Delta C_p(T - T^\circ) - T\left(\frac{\Delta H_u^\circ(T)}{T^\circ} + \Delta C_p\left(\ln\frac{T}{T^\circ}\right) + R \ln K_u(T^\circ)\right) \quad (4)$$

where $K_u(T^\circ) = 1.66pt$ for a dimer, $K_u(T^\circ) = 6.75pt^2$ for a trimer, and $K_u(T^\circ) = 37.75pt^3$ for a tetramer (*30*, *31*).

To estimate the K_u(20 °C) for the different unfolding models, the temperature denaturation of Mad1*DN was simulated with the following equation and the roots of eqs 1−3:

$$[\Theta]_{222}(T) = P_u(T)[\Theta]^u_{222}(T) + (1 - P_u(T))[\Theta]^n_{222}(T) \quad (5)$$

where $[\Theta]^u_{222}(T)$ and $[\Theta]^n_{222}(T)$ are the temperature-dependent baselines for the CD signal of the unfolded and native states, respectively. This was achieved by fixing ΔC_p to 600 kcal K mol^{-1} and optimizing the fit by varying T° and $\Delta H^\circ(T^\circ)$ as described elsewhere (*26*). The K_u values for the dimeric, trimeric, and tetrameric models have been determined to be 6.41×10^{-6}, 7.58×10^{-10}, and 8.76×10^{-16}, respectively. Once the K_u(20 °C) is determined for the different models, the only variable left is pt. The population of the different oligomers $(1 - P_u(K_u(20\ °C),pt)$ can be calculated, and the concentration dependence of the CD signal, $[\Theta]_{222}(pt)$, can be simulated in conjunction with the model-dependent expression of P_u and the following equation:

$$[\Theta]_{222}(pt) = (1 - P_u(K_u(20\ °C),pt))([\Theta]^n_{222}(20\ °C) - [\Theta]^u_{222}(20\ °C)) + [\Theta]^u_{222}(T) \quad (6)$$

The molar ellipticity for the unfolded $[\Theta]^u_{222}$(20 °C) and oligomeric $[\Theta]^n_{222}$(20 °C) states were −3 416 and −12 210 deg·cm^2·dmol^{-1}, respectively.

We show in Figure 6 the experimental $[\Theta]_{222}(pt)$ of Mad1*DN (●) at pH 6.8 and 20 °C as well as the three model-dependent simulations. As one can observe, the $[\Theta]_{222}(pt)$ is well-described by the folding of a dimer (solid black line) and that neither a trimer (solid gray line) or a tetramer (dashed line) can account for the concentration dependency observed. This result clearly demonstrates that Mad1*DN does not form a higher order oligomer and is well-described by a partially folded dimer at 20 °C. As discussed above, this was expected by the presence of Asn 112 a in the LZ domain. For comparison, we present in this figure the $[\Theta]_{222}(pt)$ of Mad1*WT (○). There is a slight residual concentration dependence, suggestive of the existence possibility of some residual quaternary (dimeric) structure.

Table 2: Thermodynamic Parameters Obtained from the Temperature-Induced Denaturation Simulations of Mad1*DN at pH 6.8 and 2.8[a]

pH 6.8				pH 2.8			
parameters		20 °C	37 °C	parameters		20 °C	37 °C
T_i°	−3.00 °C			T_i°	−3.00 °C		
T_u°	29.90 °C			T_u°	34.00 °C		
ΔH_i°	36.20 kcal/mol			ΔH_i°	45.20 kcal/mol		
ΔH_u°	44.28 kcal/mol			ΔH_u°	73.31 kcal/mol		
ΔG_u° (kcal/mol)		7.02	4.90	ΔG_u° (kcal/mol)		8.75	5.32
K_D		5.83×10^{-6}	3.54×10^{-4}	K_D		2.98×10^{-7}	1.77×10^{-4}

[a] These parameters were obtained from the temperature-induced denaturation simulations using model 3 (Figure 5b) and were used to generate the different populations as described elsewhere (*26*) and as shown in parts b and c of Figure 4.

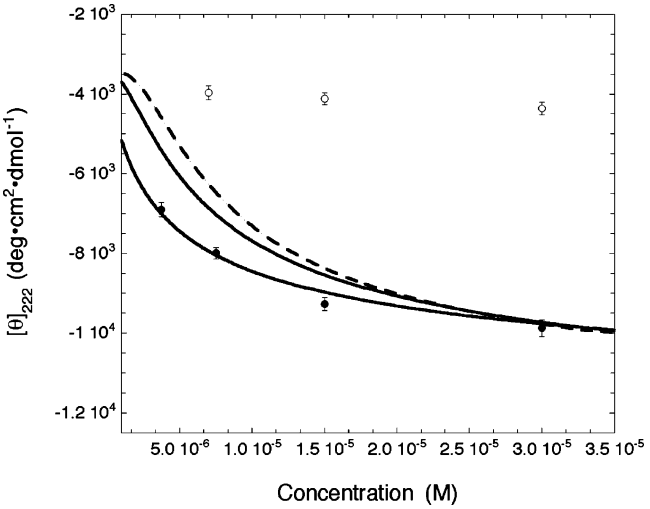

FIGURE 6: $[\Theta]_{222}(pt)$ for three model-dependent simulations of the temperature-induced denaturation using equation $[\Theta]_{222}(pt) = (1 - P_u(K_u(20\ °C),pt))([\Theta]^n_{222}(20\ °C) - [\Theta]^u_{222}(20\ °C)) + [\Theta]^u_{222}(T)$. Simulations of a dimer (solid black line), trimer (solid gray line), and tetramer (dashed line) were performed using the K_u value of 6.41×10^{-6}, 7.58×10^{-10}, and 8.76×10^{-16}, respectively. Experimental $[\Theta]_{222}(pt)$ at pH 6.8 and 20 °C is shown as ○ for Mad1*WT and ● for Mad1*DN.

For the sake of completeness, we show in Figure 5a the far-UV CD spectrum of Mad1*DN at 20 °C and pH 2.8 (●) as well as the temperature denaturation recorded at pH 2.8 in Figure 5b (●). The CD spectrum, the thermodynamical parameters, the temperature denaturation, and the population states (Figure 4c) are nearly indistinguishable from those of Mad1*WT recorded under the same conditions. This indicates that Asp112 a is most likely protonated at pH 2.8 and engaged in interfacial side-chain/side-chain hydrogen bonds in a fashion similar to that reported earlier for Asn side chains at position a of LZ domains (*28*). In summary, our results demonstrate that Asp112 a, with its negative charge at pH 6.8, is responsible for the lack of a significant dimerization of Mad1 b-HLH-LZ and that its protonation at low pH or its replacement by the isosteric and polar side chain of Asn enables the significant population of dimeric species of the b-HLH-LZ.

*Mad1*DN Can Form a Stable Complex with an E-Box dsDNA Sequence at Physiological Temperature.* As reported earlier (*6*), Mad1 cannot bind DNA as a homodimer under physiological conditions. It is thought that it necessarily needs to heterodimerize with Max to do so. As discussed elsewhere (*25*), the mechanism of specific DNA binding by dimeric b-HLH-LZ consists of the stabilization of pre-existing competent binding states with at least the HLH and the last helical turn of the basic region folded to fit into the E-box major grooves. Therefore, the inability of Mad1 to bind DNA as a homodimer could either be the result of an intrinsic inability of the Mad1 homodimer to make favorable interactions with DNA or simply that under physiological conditions there is not enough homodimeric Mad1 with the minimal structural requirement to bind DNA. In this regard, Mad1*DN should have a higher propensity than Mad1*WT to bind DNA. Moreover, testing the ability of Mad1*DN to bind DNA would help to characterize the nature of the partially folded dimer. Indeed, DNA binding by Mad1*WT and Mad1*DN would proceed if a DNA competent binding homodimeric state population, with the HLH folded, is present. In this context, we have undertaken the characterization of the relative abilities of Mad1*WT and Mad1*DN to bind E-box dsDNA by CD and EMSA.

We present in Figure 7a the far-UV CD spectra of Mad1*WT and Mad1*DN in the presence of a slight excess of E-box dsDNA at 20 °C. α-Helical content is stabilized for both, Mad1*WT and Mad1*DN, suggesting that even Mad1*WT (○), apparently devoid of a significant quaternary structure, binds DNA at 20 °C. To verify the specific nature of the DNA complexes formed, we have performed an EMSA using a radio-labeled E-box dsDNA probe in the presence of a 30-fold excess of competitive and nonspecific DNA (inset of Figure 7a; lanes 2 and 3 correspond to Mad1*WT and Mad*DN, respectively). As one can see, both b-HLH-LZ retarded the probe confirming the specific nature of DNA binding and that b-HLH dimeric states are transiently folded and stabilized by DNA for both Mad1*WT and Mad1*DN at 20 °C.

The $[\Theta]_{222}$ of −13 000 deg·cm^2·dmol^{-1} of Mad1*WT in the presence of DNA corresponds to approximately 50% of the helical content of a fully folded complex between the b-HLH-LZ of Max and an E-box dsDNA (−27 000 deg·cm^2·dmol^{-1}) (*26*). Interestingly, the b-region, H1, and H2 account for 55% of the helical content of a fully folded b-HLH-LZ/E-box dsDNA complex, supporting the existence of a stoichiometric 1:1 complex for Mad1*WT with the LZ unfolded. As stated above, this also suggests that the residual quaternary structure observed for Mad1*WT (Figure 7a, ○) could correspond to a transient population of dimeric states with the HLH folded at 20 °C, as depicted in the equilibrium to the left of Figure 8. The $[\Theta]_{222}$ of the Mad1*DN/E-box dsDNA complex is −17 000 deg·cm^2·dmol^{-1}. The additional helical content of Mad1*DN, compared to Mad1*WT, could come from the stabilization of the LZ by the mutation and suggests an equilibrium between the completely folded

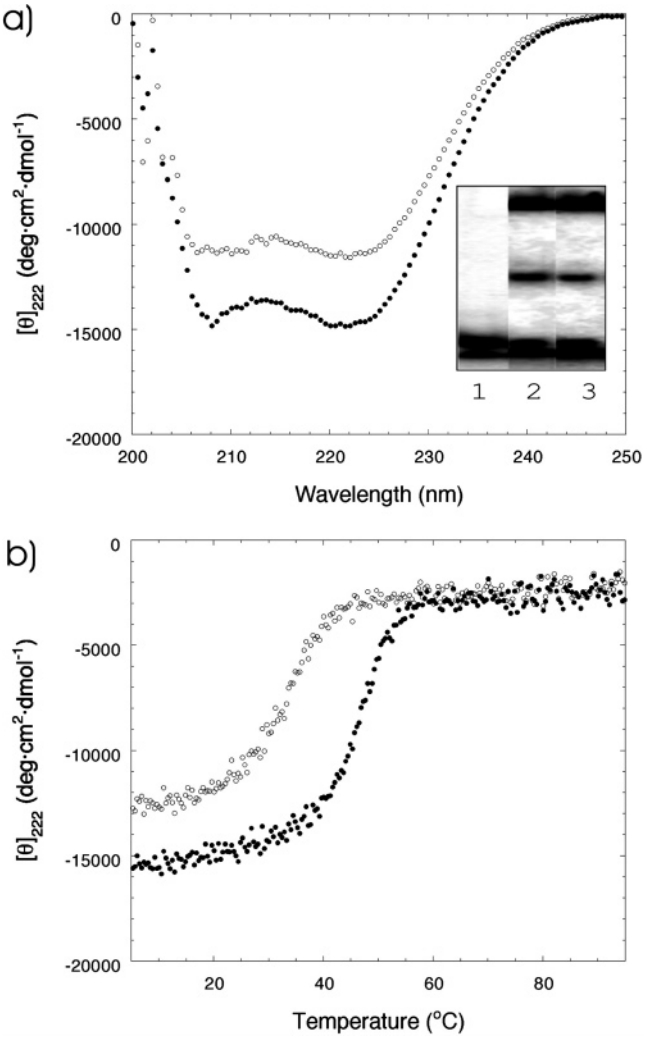

FIGURE 7: (a) Far-UV CD spectra of Mad1*WT (○) and Mad1*DN (●) in the presence of an E-box dsDNA sequence at 20 °C and pH 6.8. The data are presented in units of mean residual molar ellipticity ([Θ]): deg·cm^2·dmol^{-1}. (b) Temperature-induced denaturation monitored by recording [Θ] at 222 nm as a function of the temperature of Mad1*WT (30 μM monomer, ○) and Mad1*DN (30 μM monomer, ●) in the presence of E-box dsDNA (4 0μM single-strand units) buffered in CD buffer (50 mM phosphate, 50 mM KCl, and 5 mM DTT at pH 6.8). In the inset, we show the EMSA autoradiograph using 1.28 ng (0.2 pmol) of radio-labeled E-box dsDNA probe in the presence of 33 ng of nonspecific Herring DNA. Lane 1, probe without protein; lane 2, probe with Mad1*WT; and lane 3, probe with Mad1*DN.

b-HLH-LZ/E-box complex and b-HLH/E-box complex with the LZ unfolded as depicted in Figure 8 (equilibrium to the right). In addition, this suggests that both intermediate states (LZ folded and HLH unfolded and vice versa) are populated at 20 °C in the absence of DNA as depicted at the bottom of Figure 8. If the DNA stabilizes pre-existing binding competent states, no complex between Mad1*WT and the E-box should be detectable at 37 °C, where the Mad1*WT has no apparent residual quaternary structure (Figure 2b). To assess this premise, we have performed a temperature denaturation of Mad1*WT/E-box dsDNA complexes (Figure 7b). The results obtained show that the Mad1*WT/E-box dsDNA complex has an apparent $T°$ of approximately 32 °C and is completely disrupted at approximately 38 °C as indicated by the end of the transition and the $[\Theta]_{222}$ of −4 400 deg·cm^2·dmol^{-1} (○), which is near the $[\Theta]_{222}$ of the

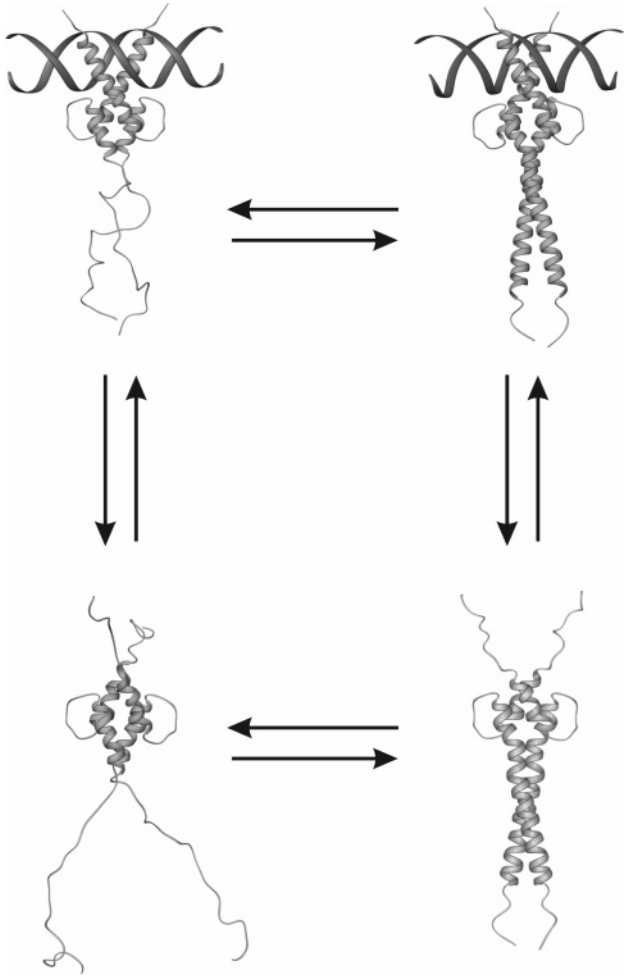

FIGURE 8: Specific DNA-binding mechanism by Mad1*WT and Mad1*DN. The binding of Mad*WT to DNA is proposed to proceed through a transient population of a partially folded dimer with the HLH folded. A similar mechanism is proposed for Mad1*DN, with the only difference that the DNA binding could proceed through the folded b-HLH-LZ at low temperature.

denatured Mad*WT (Figure 2b). This suggests that no Mad1*WT/E-box dsDNA complex exists at 37 °C, 30 μM, and pH 6.8. It is important to remember that the contribution of the E-box dsDNA was subtracted from the Mad1*WT and DN/E-box dsDNA complex spectra and denaturations and that the $T°$ of the E-box dsDNA is 78 °C (*26*). Conversely, one can clearly see that the Mad1*DN/E-box dsDNA complex is more stable and is still formed at 37 °C with an apparent $T°$ of approximately 47 °C (Figure 7b, ●).

Overall, these results demonstrate that Mad1 homodimeric b-HLH can form a favorable interaction with the E-box DNA sequence and that the inability of Mad1*WT to bind DNA under physiological condition is rather linked to its deficiency to populate in pre-existing DNA-binding competent states under physiological conditions of temperature. Asp 112 a plays a major role in this deficiency.

DISCUSSION

Similar to all of the members of the Max-interacting b-HLH-LZ transcription-factor family, Mad1 is not able to form a homodimer nor bind DNA alone (*6*). Mad1 has to heterodimerize with Max to bind DNA and repress the transcription of c-Myc target genes. The inability of Mad1

to form a homodimer plays an intrinsic part in the mechanism of specific heterodimerization with Max. In fact, it has been hypothesized that key conserved acidic residues at the interface of all of the Myc and Mad proteins (Figure 1a) are responsible for the destabilization of the homodimers and would form specific and stable interactions at the interface of the heterodimers with Max (*16*, *17*, *25*, *26*).

We have shown here that the b-HLH-LZ of Mad1 does not form quaternary interactions nor binds DNA at 30 μM and 37 °C. The single replacement of the conserved acidic side chain at position a in the LZ (Asp 112) is sufficient to induce the formation of b-HLH-LZ dimeric states and allows the formation of a stable E-box dsDNA complex at 37 °C. This clearly establishes Asp112 a as a key residue for the destabilization of Mad1 and validates our hypothesis that the acidic side chains conserved at this position play a conserved role in the destabilization of all of the Max-interacting partners. On the other hand, Nair and Burley have suggested that the single Glu 125 g of the LZ of Mad1 (Figure 1b) is responsible for the destabilization of the homodimer (*19*). Our results suggest that Glu 125 g is not the sole residue involved in the destabilization of the Mad1 homodimer and in fact may not be an important determinant. Indeed, if this were the case, the mutation of Asp 112 for an Asn would not have had the effect of triggering homodimerization. In addition, inspection of the helical-wheel diagrams of the Mad1 homodimeric and heterodimeric LZ (parts b and c of Figure 1, respectively) as well the X-ray structure of the heterodimeric Mad1/Max b-HLH-LZ/E-box dsDNA complex suggest that Glu 125 g is likely to be involved in solvent-exposed and favorable g and e′ (i, i′ + 5) electrostatic interactions with Lys 130 e at the interface of the Mad1 homodimer and in an unfavorable repulsion with Max Glu 96 e at the interface of the heterodimer, respectively. It is therefore difficult to reconcile these observations with the fact that this residue could be involved in the destabilization of the homodimeric b-HLH-LZ. On the other hand, Asp 112 a would have to be directly buried at the interface of the homodimeric LZ. As reported elsewhere, the burial of a charged carboxylate at this position leads to severe repulsions and unfavorable desolvation effects in homodimers (*16*−*17*). According to the knobs into holes model, Asp 112 a could be engaged in favorable electrostatic interactions with His 81 d at the interface of the heterodimeric Mad1/Max LZ. In fact, the crystal structure of the heterodimeric Mad1/Max/E-box complex reveals that Asp 112 a of Mad1 and His 81 d of Max are within 4 Å of each other and are most likely to be involved in favorable electrostatic interactions as predicted.

The existence of such stable interactions between the homologous Glu 410 a of c-Myc and His 81 d of Max have been demonstrated by pK_a measurements and the solution structure of the heterodimeric c-Myc/Max LZ (*16*−*17*). This interaction is also observed in the crystal structure of the c-Myc/Max heterodimeric/E-box complex (*19*).

In conclusion, the results presented here support the premise that Asp 112 a of Mad1 is a crucial residue for the molecular recognition between the b-HLH-LZ of Mad1 and Max by destabilizing the homodimeric b-HLH-LZ of Mad1 and forming favorable interactions at the interface of the heterodimer. More generally, our results support the hypothesis that acidic residues conserved at the interface of the LZ (Figure 1a) of all of the members of Mad and Myc family are involved in a conserved mechanism of molecular recognition by destabilizing homodimers and allowing for the formation of a specific interaction with the peculiar interfacial His residue on Max.

ACKNOWLEDGMENT

The authors are grateful to R. N. Eisenman, Fred Hutchinson Cancer Research Center, Seattle, WA, for the pME18S-Mad1 plasmid.

REFERENCES

1. Amati, B., and Land, H. (1994) Myc-Max-Mad: A transcription factor network controlling cell cycle progression, differentiation, and death, *Curr. Opin. Genet. Dev. 4*, 102−108.
2. Hurlin, P. J., Ayer, D. E., Grandori, C., and Eisenman, R. N. (1994) The Max transcription factor network: Involvement of Mad in differentiation and an approach to identification of target genes, *Cold Spring Harbor Symp. Quant. Biol. 59*, 109−116.
3. Luscher, B. (2001) Function and regulation of the transcription factors of the Myc/Max/Mad network, *Gene 277*, 1−14.
4. Oster, S. K., Ho, C. S., Soucie, E. L., and Penn, L. Z. (2002) The myc oncogene: marvelously complex, *Adv. Cancer Res. 84*, 81−154.
5. Blackwood, E. M., and Eisenman, R. N. (1991) Max: A helix−loop−helix zipper protein that forms a sequence-specific DNA-binding complex with Myc, *Science 251*, 1211−1217.
6. Ayer, D. E., Kretzner, L., and Eisenman, R. N. (1993) Mad: A heterodimeric partner for Max that antagonizes Myc transcriptional activity, *Cell 72*, 211−222.
7. Chin, L., Schreiber-Agus, N., Pellicer, I., Chen, K., Lee, H. W., Dudast, M., Cordon-Cardo, C., and DePinho, R. A. (1995) Contrasting roles for Myc and Mad proteins in cellular growth and differentiation, *Proc. Natl. Acad. Sci. U.S.A. 92*, 8488−8492.
8. Hurlin, P. J., Foley, K. P., Ayer, D. E., Eisenman, R. N., Hanahan, D., and Arbeit, J. M. (1995) Regulation of Myc and Mad during epidermal differentiation and HPV-associated tumorigenesis, *Oncogene 11*, 2487−2501.
9. Grandori, C., Cowley, S. M., James, L. P., and Eisenman, R. N. (2000) The Myc/Max/Mad network and the transcriptional control of cell behavior, *Annu. Rev. Cell Dev. Biol. 16*, 653−699.
10. McMahon, S. B., Wood, M. A., and Cole, M. D. (2000) The essential cofactor TRRAP recruits the histone acetyltransferase hGCN5 to c-Myc, *Mol. Cell Biol. 20*, 556−562.
11. Zhang, W., Bone, J. R., Edmonston, D. G., Turner, B. M., and Roth, S. Y. (1998) Essential and redundant functions of histone acetylation revealed by mutation of target lysines and loss of the Gcn5p aceltyltransferase, *EMBO J. 17*, 3155−3167.
12. Sommer, A., Hilfenhaus, S., Menkel, A., Kremmer, E., Seiser, C., Loidl, P., and Luscher, B. (1997) Cell growth inhibition by the Mad/Max complex through recruitment of histone deacetylase activity, *Curr. Biol. 7*, 357−365.
13. Ayer, D. E., Lawrence, Q. A., and Eisenman, R. N. (1995) Mad-Max transcriptional repression is mediated by ternary complex formation with mammalian homologs of yeast repressor Sin3, *Cell 80*, 767−776.
14. Laherty, C. D., Yang, W. M., Sun, J. M., Davie, J. R., Seto, E., and Eisenman, R. N. (1997) Histone deacetylases associated with the mSin3 corepressor mediate mad transcriptional repression, *Cell 89*, 349−356.
15. Sommer, A., Bousset, K., Kremmer, E., Austen, M., and Luscher, B. (1998) Identification and characterization of specific DNA-binding complexes containing members of the Myc/Max/Mad network of transcriptional regulators, *J. Biol. Chem. 273*, 6632−6642.
16. Lavigne, P., Kondejewski, L. H., Houston, M. E., Jr., Sonnichsen, F. D., Lix, B., Skyes, B. D., Hodges, R. S., and Kay, C. M. (1995) Preferential heterodimeric parallel coiled-coil formation by synthetic Max and c-Myc leucine zippers: A description of putative electrostatic interactions responsible for the specificity of heterodimerization, *J. Mol. Biol. 254*, 505−520.
17. Lavigne, P., Crump, M. P., Gagne, S. M., Hodges, R. S., Kay, C. M., and Sykes, B. D. (1998) Insights into the mechanism of

heterodimerization from the ^{1}H NMR solution structure of the c-Myc-Max heterodimeric leucine zipper, *J. Mol. Biol. 281*, 165−181.
18. Ciarapica, R., Rosati, J., Cesareni, G., and Nasi, S. (2003) Molecular recognition in helix−loop−helix and helix−loop−helix−leucine zipper domains. Design of repertoires and selection of high affinity ligands for natural proteins, *J. Biol. Chem. 278*, 12182−12190.
19. Nair, S. K., and Burley, S. K. (2003) X-ray structures of Myc-Max and Mad-Max recognizing DNA. Molecular bases of regulation by proto-oncogenic transcription factors, *Cell 112*, 193−205.
20. Ferre-D'amare, A. R., Predengrast, G. C., Ziff, E. B., and Burley, S. K. (1993) Recognition by Max of its cognate DNA through a dimeric b/HLH/Z domain, *Nature 363*, 38−45.
21. Carson, M. (1987) Ribbon models of macromolecules, *J. Mol. Graphics 5*, 103−106.
22. Lavigne, P., Sonnichsen, F. D., Kay, C. M., and Hodges, R. S. (1996) Interhelical salt bridges, coiled-coil stability, and specificity of dimerization, *Science 271*, 1136−1138.
23. Wagschal, K., Tripet, B., Lavigne, P., Mant, C., and Hodges, R. S. (1999) The role of position a in determining the stability and oligomerization state of α-helical coiled coils: 20 amino acid stability coefficients in the hydrophobic core of proteins, *Protein Sci. 8*, 2312−2329.
24. Tripet, B., Wagschal, K., Lavigne, P., Mant, C. T., and Hodges, R. S. (2000) Effects of side-chain characteristics on stability and oligomerization state of a *de novo*-designed model coiled-coil: 20 amino acid substitutions in position "d", *J. Mol. Biol. 300*, 377−402.
25. Sauve, S., Tremblay, L., and Lavigne, P. (2004) The NMR solution structure of a mutant of the Max b/HLH/LZ free of DNA: Insights into the specific and reversible DNA binding mechanism of dimeric transcription factors, *J. Mol. Biol. 342*, 813−832.
26. Naud, J. F., Gagnon, F., Wellinger, R. J., Chabot, B., and Lavigne, P. (2003) Improving the thermodynamic stability of the leucine zipper of max increases the stability of its b-HLH-LZ:E-box complex, *J. Mol. Biol. 326*, 1577−1595.
27. Gonzalez, L., Jr., Woolfson, D. N., and Alber, T. (1996) Buried polar residues and structural specificity in the GCN4 leucine zipper, *Nat. Struct. Biol. 3*, 1011−1018.
28. Junius, F. K., Mackay, J. P., Bubb, W. A., Jensen, S. A., Weiss, A. S., and King, G. F. (1995) Nuclear magnetic resonance characterization of the Jun leucine zipper domain: Unusual properties of coiled-coil interfacial polar residues, *Biochemistry 34*, 6164−6174.
29. Zhu, H., Celinski, S. A., Scholtz, J. M., and Hu, J, C. (2001) An engineered leucine zipper a position mutant with an unusual three-state unfolding pathway, *Protein Sci. 10*, 24−33.
30. Yu, Y. B., Lavigne, P., Kay, C. M., Hodges, R. S., and Privalov, P. L. (1999) Contribution of translational and rotational entropy to the unfolding of a dimeric coiled-coil, *J. Phys. Chem. B 103*, 2270−2278.
31. Jelesarov, I., and Lu, M. (2001) Thermodynamics of trimer-of-hairpins formation by the SIV gp41 envelope protein, *J. Mol. Biol. 307*, 637−656.

BI0500731